Andean Geology 49 (3): 313-326. September, 2022
doi: 10.5027/andgeoV49n3-3402

Andean Geology
www.andeangeology.cl

(U-Th)/He ages of Proterozoic-Paleozoic basement rocks from northern Chile (18-19° S) and implications on the Neogene uplift history of the Western Cordillera

Marcelo García[1, 2], *Germán Aguilar[1], María Pía Rodríguez[3], James Metcalf[4]

[1] *Advanced Mining Technology Center, Universidad de Chile, Av. Tupper 2007, Santiago, Chile. mgarciagodoy@ing.uchile.cl; german.aguilar@amtc.cl*

[2] *Departamento de Geología, Universidad de Chile, Plaza Ercilla 803, Santiago, Chile.*

[3] *Departamento de Geología, Universidad de Atacama, Copayapu 485, Copiapó, Atacama, Chile. mariapia.rodriguez@uda.cl*

[4] *Department of Geological Sciences, University of Colorado, Boulder, 2200 Colorado Ave, UCB 399, CO 80309, United States. james.metcalf@colorado.edu*

** Corresponding author: german.aguilar@amtc.uchile.cl*

ABSTRACT. In the Western Cordillera of northern Chile, the Proterozoic-Paleozoic Belén Metamorphic Complex is covered by late Oligocene-early Miocene (25-18 Ma) rocks, and both units are involved in west-vergent contractional deformation, which results in exhumation. A Miocene age (18 to 6 Ma) for deformation has been previously constrained by stratigraphy and cross-cutting relationships. To understand the youngest exhumation event and reverse faulting, we obtained 21 (U-Th)/He ages from two samples of the metamorphic rocks and the associate inverse thermal modeling. Five zircon (U-Th)/He ages from one sample are 113 to 226 Ma, very scattered, while five zircon ages from the other, are 20 to 49 Ma. The high dispersion of zircon (U-Th)/He data prevents the geological interpretation of results. Apatite grains from both samples yielded 11 (U-Th)/He ages between 10.4 and 18.7 Ma, with 9 values from 12.0 to 15.5 Ma. A slight positive correlation between apatite single-grain dates and effective uranium for 4 crystals of one sample suggests relatively slow cooling. The T-t model including these 4 apatite ages shows continuous cooling from 15 to 0 Ma with a relatively more marked cooling period at 11-7 Ma. The middle-late Miocene thermal signal agrees with the geologic evolution of the region and would permit to date the last activity of the Chapiquiña-Belén reverse fault, which uplifted and exhumed the metamorphic rocks. This signal is relatively similar to that the eastern Altiplano, but differs considerably from that the forearc.

Keywords: Andean uplift, Basement rocks, (U-Th)/He ages, Zircon, Apatite.

RESUMEN. Edades (U-Th)/He de rocas del basamento proterozoico-paleozoico del norte de Chile (18-19° S) e implicancias sobre la historia del alzamiento neógeno de la Cordillera Occidental. En la Cordillera Occidental del norte de Chile, el Complejo Metamórfico de Belén del Proterozoico-Paleozoico está cubierto por rocas del Oligoceno superior-Mioceno inferior (25-18 Ma), y ambas unidades están involucradas en un proceso de deformación contraccional con vergencia al oeste, que produce exhumación. Con base en la estratigrafía y las relaciones de corte se ha establecido previamente una edad miocena (18 a 6 Ma) para la deformación. Con la finalidad de entender el evento de exhumación más joven y de fallamiento inverso, obtuvimos 21 edades (U-Th)/He de dos muestras de las rocas metamórficas y realizamos el modelamiento termal asociado. Cinco edades (U-Th)/He en circones de una de las muestras resultaron muy dispersas (de 113 a 226 Ma), mientras que cinco edades en circones de la otra muestra varían entre 20 y 49 Ma. La alta dispersión de los datos (U-Th)/He en circón impide la interpretación geológica de los resultados. Los granos de apatito de las dos muestras permitieron la obtención de 11 edades (U-Th)/He entre 10,4 y 18,7 Ma, con 9 valores comprendidos entre 12,0 y 15,5 Ma. Una moderada correlación positiva entre las edades de granos individuales de apatito y el uranio efectivo para 4 cristales de una de las muestras estudiadas sugiere un enfriamiento relativamente lento. El modelo T-t, incluyendo estas 4 edades en apatito, muestra un enfriamiento continuo de 15 a 0 Ma, con un período de enfriamiento relativamente más marcado a los 11-7 Ma. La señal termal miocena media-tardía se corresponde con la evolución geológica de la región y permitiría datar la última actividad de la falla Chapiquiña-Belén, la que levantó y exhumó las rocas metamórficas. Esta señal es relativamente similar a aquella del Altiplano oriental, pero difiere considerablemente de la del antearco.

Palabras clave: Alzamiento andino, Rocas de basamento, Edades (U-Th)/He, Circón, Apatito.

1. Introduction

Thermo-chronological data are usually utilized to track the cooling/exhumation of basement rocks, and sampling surveys must have the availability to measure temperature changes in the older rocks (Murray *et al*., 2018). In the eastern portion of the Altiplano plateau (14-22° S), the basement is mainly Paleozoic in age and largely exposed, and abundant fission-track and (U-Th)/He data therein indicate major exhumation events in the Eocene-Oligocene (40-25 Ma) and Miocene (20-2 Ma) (Gillis *et al*., 2006; Ege *et al*., 2007; McQuarrie *et al*., 2008; Barnes *et al*., 2012; Perez *et al*., 2016; Anderson *et al*., 2018). In the western Altiplano, volcanic and sedimentary Cenozoic rocks are dominant (Fig. 1) and the geologic evolution indicates major deformation and uplift during the Eocene Incaic orogeny and Miocene Quechua orogeny (Charrier *et al.*, 2013; García *et al.*, 2017). In the Western Cordillera, older rocks are locally exposed and their thermochronological record is poor, whereas in the forearc (from the Coastal Cordillera to Chilean Precordillera), the basement is Jurassic-Paleocene in age and their thermochronological data are largely older than 24 Ma (Fig. 1) and indicate very slow exhumation since the Cretaceous (Schlunegger *et al*., 2006; Schildgen *et al*., 2007; Avdievitch *et al*., 2018).

Two outcrops of Proterozoic-Paleozoic metamorphic rocks occur in the Western Cordillera at 18-19° S, the Uyarani and Belén complexes (Fig. 1). In westernmost Bolivia (Uyarani), apatite fission-track (AFT) and apatite (U-Th)/He (AHe) data in Proterozoic rocks suggest mostly Eocene cooling (Horton *et al*., 2006; Barnes *et al*., 2012). In the Proterozoic-Paleozoic Belén Metamorphic Complex (BMC) of northernmost Chile (Figs. 1 and 2; Salas *et al*., 1966; Wörner *et al*., 2000a; García *et al*., 2004; Charrier *et al*., 2013), the thermochronological record consists of one zircon fission-track age of 75±5 Ma (Damm *et al*., 1994) and AFT and AHe ages of 11-13 Ma (Horton *et al*., 2006). Analytical data, errors and sample locations are not reported, and thermal modeling not developed for the BMC rocks. Zircon (U-Th)/He (ZHe) data are not available today. The AFT and AHe ages were interpreted as provoked by rapid cooling (Horton *et al*., 2006) or thermal reset (Wotzlaw *et al*., 2011).

The Western Cordillera at 18-19° S, in northernmost Chile, is affected by Neogene west-vergent faulting and folding, which have been dated from 18 to 6 Ma, according to cross-cutting relationships and absolute age of syn-kinematic sequences (García *et al*., 2004; Charrier *et al*., 2013). This age range is consistent with the today available AFT and AHe ages for the Proterozoic-Paleozoic BMC rocks; however, the Chilean Precordillera is also affected by Neogene deformation and the AFT and AHe data in the basement rocks are older than 24 Ma (Cretaceous-Paleogene), similar to that the Coastal Cordillera. As the Western Cordillera deformation involves the BMC rocks, combined zircon/apatite He ages

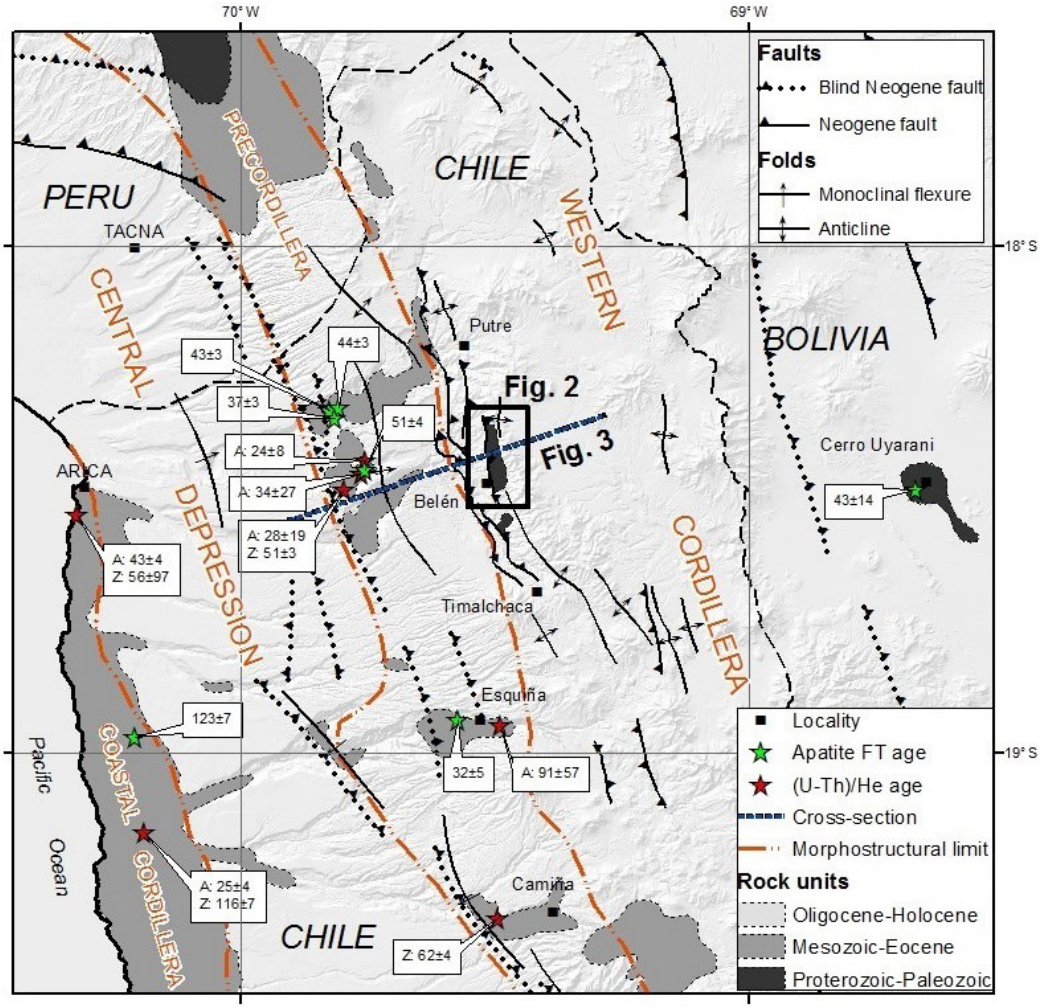

FIG. 1. Simplified geological map of the northernmost Chile, westernmost Bolivia and southernmost Peru showing distribution of rock units, main structures, morpho-structural domains, available thermochronological ages (in Ma), and location of the figure 2 (Belén area) and figure 3 (structural cross-section). Geology based on maps of the Geological Surveys of Chile, Bolivia and Peru. Proterozoic-Paleozoic rocks are metamorphic, Mesozoic-Eocene rocks are igneous and sedimentary, and Oligocene-Holocene units are continental volcanic and sedimentary rocks and unconsolidated deposits. Note the absence of Proterozoic to Eocene bedrock outcrops in the Western Cordillera. Thermochronological ages are previous to this study. (U-Th)/He ages are from Avdievitch *et al.* (2018). Apatite fission-track ages are from Schlunegger *et al*. (2006) in Chile and Barnes *et al*. (2012) in Bolivia. Some zircon and apatite fission-track ages and AHe ages are reported in the Belén and Uyarani areas, but their sample locations and other details are unknown (see text).

on these rocks would permit to track their youngest cooling history, and infer an absolute age for the last activity of the fault that uplift the BMC rocks. In order to contribute on the understanding of these topics, we present and discuss new 10 ZHe ages and 11 AHe ages from two samples of the BMC, and we develop inverse T-t models obtained with these ages and geological constraints.

2. Geological setting

2.1. Stratigraphy

The BMC consists of two lithologic units, one of amphibolites, schists and gneisses, and one of granitic orthogneisses (Fig. 2; *e.g.*, García *et al*., 2004). Numerous and diverse isotopic ages have

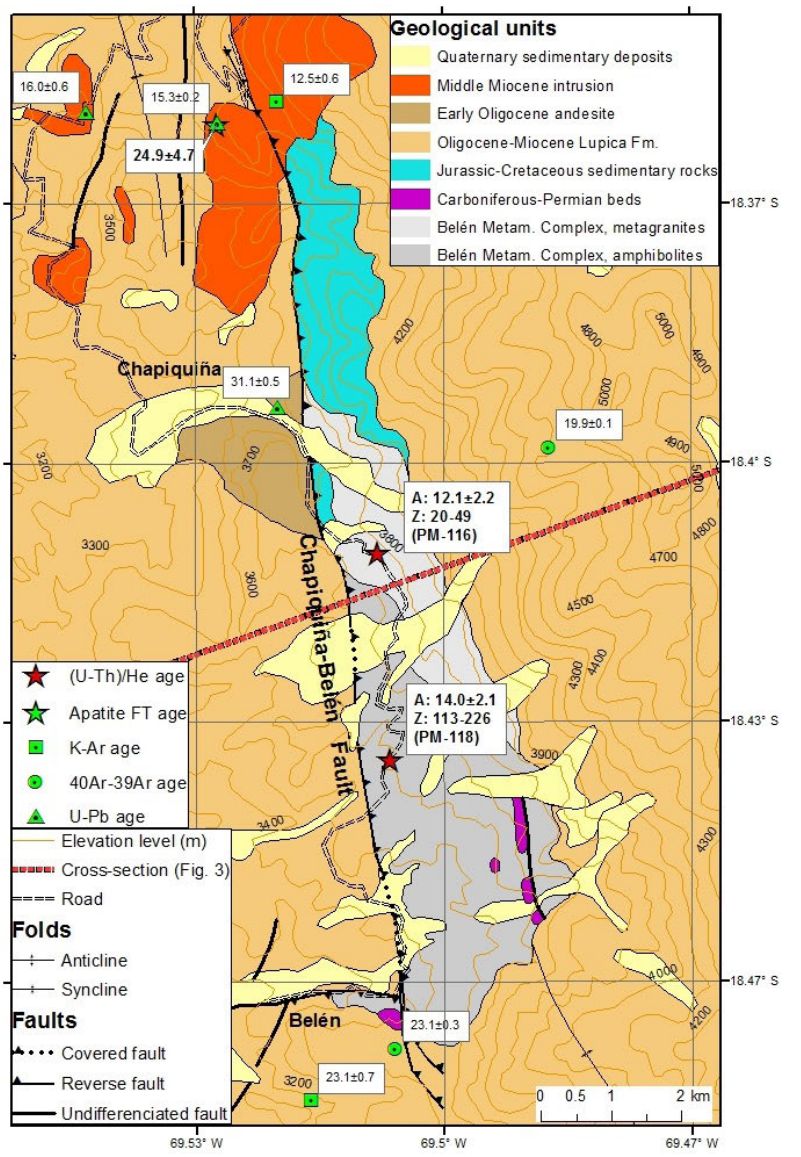

FIG. 2. Geological map of the Belén area in northernmost Chile at *ca*. 18.5° S, showing location and results of the samples analyzed; map based on García *et al*. (2004) and Arcos *et al*. (2016). The geochronological and thermo-chronological ages are in Ma. For the new (U-Th)/He ages: A, apatite and Z, zircon. For the AHe ages, the mean weighted values are indicated (see text), whereas for the ZHe ages, the value ranges. The U-Pb, $^{40}Ar/^{39}Ar$ and K-Ar ages are from Muñoz and Charrier (1996), Wörner *et al*. (2000b), García *et al*. (2004) and Arcos *et al.* (2016), and the apatite fission-track age from Schlunegger *et al*. (2006). For the BMC rocks, available isotopic ages are not showed for simplification (see text).

been interpreted as related to protolith formation or metamorphism and intrusion events. Concerning the metamorphism age, two Rb-Sr isochrons on schists indicated *ca*. 1,000 Ma and *ca.* 544 Ma values, respectively (*i.e*., Proterozoic to early Paleozoic; Pacci *et al*., 1980; Basei *et al*., 1996). Several U-Pb zircon dates, from 473±3 to 366±3 Ma, have been considered as magmatic-crystallization ages (of the protolith units) and metamorphism ages (Wörner *et al*., 2000a; Loewy *et al*., 2004; Arcos *et al*., 2016. In fact, duplicates of the same samples analyzed by (U-Th)/He in this work (PM-116 and PM-118)

have been dated by U-Pb zircon (Arcos *et al*., 2016): the major zircon populations from two samples gave 472±2 and 465±2 Ma, respectively, and were interpreted as magmatic-protolith ages, whereas alternative-minor zircon populations gave 444±4 and 442±4 Ma, respectively, and were considered as related to high-temperature metamorphism events (Arcos *et al*., 2016).

The BMC is locally overlain unconformably by Carboniferous-Permian sedimentary rocks and Jurassic-early Cretaceous marine sedimentary rocks (Fig. 2; Wörner *et al*., 2000a; García *et al*., 2004). These three units are largely covered in angular unconformity by *ca.* 2,500 m thickness of continental volcanic and sedimentary rocks of the Lupica Formation, which consists roughly of a lower unit of andesitic-dacitic lavas and breccias, a middle unit of rhyolitic tuffs, and an upper unit of sandstones and lacustrine rocks (García *et al.*, 2004). The formation has a late Oligocene to early Miocene age (25-18 Ma), according to numerous U-Pb, $^{40}Ar/^{39}Ar$, and K-Ar determinations (Wörner *et al*., 2000b; García *et al*., 2004; Arcos *et al*., 2016). In Chapiquiña, this unit overlays an andesite lava dome, which has been dated by U-Pb zircon at 31.1±0.5 Ma (early Oligocene; Arcos *et al*., 2016). The depositional contact relationship between the BMC and Lupica Formation indicate that the first was exposed to erosion prior to 25 Ma (*i.e*., during the Oligocene). In addition, clasts of the BMC in conglomerates of the Oligocene (35-23 Ma) Azapa Formation (García *et al*., 2004), and provenance studies based on heavy mineral analysis (Pinto *et al*., 2007) and detrital zircon U-Pb ages on sandstones of the Azapa Formation (Wotzlaw *et al*., 2011) also evidence an Oligocene exposition of the BMC rocks.

The Lupica Formation rocks are intruded by middle Miocene monzodioritic-dioritic stocks, with available U-Pb and K-Ar ages from 17.5±0.2 to 12.5±0.6 Ma (Muñoz and Charrier, 1996; García *et al*., 2004; Arcos *et al*., 2016). For the Miocene intrusion north of Chapiquiña, one AFT age of 25±5 Ma has been reported by Schlunegger *et al*. (2006) (Figs. 1 and 2). This intrusion was dated at 15.3±0.2 Ma by U-Pb zircon (Arcos *et al*., 2016) almost in the same location where the AFT age was obtained; also, the intrusion was dated at 12.5±0.6 Ma by K-Ar biotite, nearby (Muñoz and Charrier, 1996). Thus, the fission-track age is inconsistent because is older than the crystallization age.

2.2. Structure

The Miocene and older rocks are involved in a 70 km long belt formed by NNW striking, west-vergent folds and reverse faults, and according to the age of deformed and non-deformed sequences, the most important shortening (*ca.* 7 km) occurred between 18 and 6 Ma (Figs. 2 and 3; García *et al*., 2004; Charrier *et al*., 2013). One of these structures is the Chapiquiña-Belén fault (ChBF), a 15 km long, N-S-trending, 50-60° east-dipping reverse fault that limits the BMC in the west (Fig. 2; García *et al*., 2004; Arcos *et al*., 2016). To the west, the footwall of this fault consists largely of gentle to moderately inclined beds of the Lupica Formation. To the east and covering the BMC, the beds of Lupica Formation dispose as a homoclinal panel with 10-30° dip to the east. The BMC is interpreted as located in the core of a major and complex fault-bend anticline of 15-20 km half-wavelength, with a detachment fault located at *ca.* 7-10 km depth (Fig. 3; García *et al*., 2004; Charrier *et al*., 2013). The anticline is faulted in the core, and has, to the west, a frontal transported syncline and two east-dipping thrusts, which are associated with two generations of syn-kinematic fluvial gravels dated at 18-15 and 12-8 Ma (García *et al*., 2004). To the west at this latitude, in the Precordillera, Miocene shortening is much less (*ca.* 100 m) and absorbed by a gentle, 50 km long fold, the Oxaya anticline (Muñoz and Charrier, 1996; García and Hérail, 2005; García *et al.*, 2017).

3. Samples and methods

The (U-Th)/He thermochronological method is used to track the cooling history of rocks below He partial retention zone, which is of ~150-220 °C for zircon (ZHe) and ~55-90 °C for apatite (AHe) (*e.g.*, Ehlers and Farley, 2003; Reiners *et al*., 2005). The two analyzed samples of the BMC were collected at a horizontal distance of 3 km between them, and located at more than 5 km from Miocene intrusions to prevent collection of samples thermally reseted by Miocene magmatism (Fig. 2). The samples are located at similar altitude and distance from the trace of the ChBF. The sample PM-116 (at 3,760 m a.s.l.) is a granodioritic orthogneiss of biotite and muscovite, with quartz, plagioclase and orthoclase. PM-118 (at 3,600 m a.s.l.) is an amphibolitic-biotitic gneiss (or amphibolite, or metadiorite), formed by

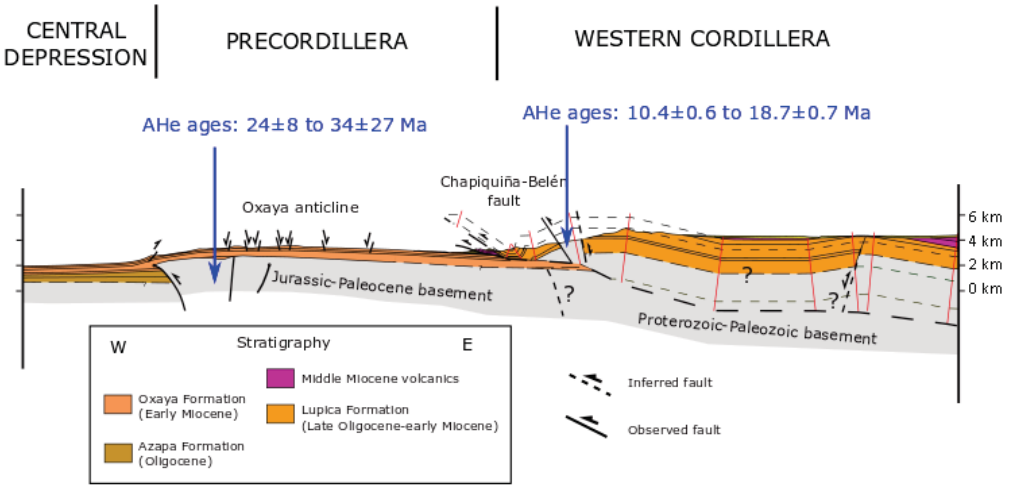

FIG. 3. Structural cross-section in the northernmost Chile Andes (modified from Charrier *et al.*, 2013), showing the main geological units and faults, as well as the available apatite (U-Th)/He ages in the basement of the Precordillera (Avdievitch *et al.*, 2018; sample mean ages) and Western Cordillera (this study; single-grain ages). Trace location of the entire cross-section in figure 1.

plagioclase, amphibole, biotite and quartz. Heavy mineral standard separation was carried out with Wilfley Table, magnetic field application and dense liquids at the laboratory of the Universidad de Chile. Zircon and apatite concentrates were obtained with binocular lens observation.

The (U-Th)/He analyses were carried out at the University of Colorado Boulder. The grains were screened for quality, including crystal size, shape and presence of inclusions. Grains were placed into Nb tubes and heated at 800-1,100 °C for He extraction and measurement line. The degassed ^{4}He is then spiked with ^{3}He and analyzed on a Balzers Prisma Plus QME 220. Grains are attack with acid combination for dissolution, and the solutions are spiked with a ^{235}U-^{230}Th-^{145}Nd tracer. Sample solutions are analyzed for U, Th, and Sm content using ICP-MS. He ages are calculated using the methods described in Ketcham *et al*. (2011). The natural occurring ^{238}U/^{235}U ratio used in data reduction is 137.818 after Hiess *et al*. (2012). Every batch of samples includes standards run sporadically, as Fish Canyon Tuff zircons and Durango fluorapatites. Additional analytic procedures can be reviewed in http://www.colorado.edu/geologicalsciences/resources/research-facilities/u-thhe-thermochronology-lab.

In order to evaluate the dispersion of data, we calculated the weighted mean ages, associated errors and MSWDs, using the Isoplot® routine for Excel® (Ludwig, 2012). To evaluate the consistency of analyses in each sample, we studied the correlation between effective uranium and calculated crystal age. (U-Th)/He measures that successfully pass this consistency tests were used to obtain inverse thermal modeling. Here we use the QTQt v 5.6.0 software (Gallagher, 2012) to model the thermal history that include the (U-Th)/He analyses in apatite (4 grains). QTQt uses a Bayesian transdimensional Markov Chain Monte Carlo method. We ran 100,000 forward models in the exploratory phase (burn in), then an additional 10,000 (post burn in) to construct the posterior distribution for the model parameters considering the data of individual samples. This is an iterative process with the proposed model being drawn from a perturbation (*i.e*., add a T-t point) of the current model. This model is either accepted, thus becoming the current model, or rejected. See Gallagher (2012) for further details on the method.

4. Results

4.1. (U-Th)/He ages

4.1.1. Sample PM-116

The five picked zircon grains of the sample PM-116 are euhedral crystals, with widths >43 µm and lengths <221 µm. Crystals show some inclusions and two terminations with slightly rounded ends (Table 1). The (U-Th)/He measures in zircon produced individual ages of 20±1, 31±2, 32±1, 35±1 and 49±1 Ma.

TABLE 1. ANALYTICAL DATA OF THE ZIRCON (U-Th)/He AGES AND CHARACTERISTICS OF THE ANALYZED GRAINS.

Full Sample Name	length 1 (µm)	width 1 (µm)	length 2 (µm)	width 2 (µm)	Np	Dim Mass (µg)	rs (µm)	^{4}He (nmol/g)	±	U (ppm)	±	Th (ppm)	±	Sm (ppm)	±	eU	^{4}He (ncc)	±	Re (%)	U (ng)	±	Th (ng)	±	Sm (ng)	±	Th/U	Raw Date it (Ma)	±	Ft	Corrected Analytic Date It (Ma)	Unc. (Ma)2σ	Notes
PM-116_z01	117.9	96.5	173.1	59.5	2	2.39	41.41	50.531	0.166	317.28	4.93	219.04	4.19	0.47	0.26	368.8	2.711	0.009	100.0	0.760	0.012	0.524	0.010	0.001	0.001	0.690	25.35	0.35	0.727	34.8	0.9	fat, euhedral crystal with two terminations, some small inclusions
PM-116_z02	203.8	85.5	203.8	64.3	2	3.90	46.49	48.771	0.154	207.45	2.33	153.55	3.09	0.38	0.21	243.5	4.267	0.014	100.0	0.810	0.009	0.599	0.012	0.001	0.001	0.740	37.02	0.38	0.755	49.0	1.0	long clear crystal, with two well-formed terminations, some inclusions
PM-116_z03	220.7	99.4	221.3	71.9	2	5.39	52.21	27.845	0.109	176.57	4.01	134.91	2.65	0.42	0.13	208.3	3.363	0.013	99.7	0.951	0.022	0.727	0.014	0.002	0.001	0.764	24.73	0.48	0.780	31.7	1.2	biggish well-formed crystal with two terminations, some inclusions
PM-116-4	152.4	49.0	142.9	43.0	2	1.14	29.95	19.923	0.079	157.03	5.54	133.80	2.48	-	188.5	188.5	0.511	0.002	99.7	0.180	0.006	0.153	0.003	-	0.852	0.852	19.56	0.57	0.631	31.0	1.8	several inclusions, clear and beautiful otherwise
PM-116-5	172.7	54.9	172.6	51.9	2	1.82	34.93	26.725	0.118	304.45	7.57	243.19	6.21	-	361.6	361.6	1.087	0.005	99.9	0.553	0.014	0.441	0.011	-	0.799	0.799	13.69	0.29	0.680	20.1	0.9	slightly rounded terminations, inclusions
PM-118_z01	233.1	117.3	233.3	117.8	2	9.95	68.67	130.751	0.377	103.51	2.75	99.09	0.91	0.27	0.09	126.8	29.155	0.084	100.0	1.030	0.027	0.986	0.009	0.003	0.001	0.957	188.19	4.00	0.830	225.9	9.6	big, slightly rounded, clear, well-defined faces, two terminations, some inclusions
PM-118_z02	292.3	98.6	298.3	86.0	2	9.21	60.03	66.936	0.157	88.08	1.37	75.63	1.18	0.48	0.14	105.9	13.810	0.032	99.6	0.811	0.013	0.696	0.011	0.004	0.001	0.859	116.09	1.51	0.807	143.5	3.8	big and long, nice faces, slightly rounded ends, euhedral, two terminations, some inclusions
PM-118_z03	268.0	115.4	264.6	125.8	2	12.54	72.66	102.461	0.188	133.26	2.80	117.99	1.95	0.36	0.09	161.0	28.797	0.053	99.4	1.671	0.035	1.480	0.024	0.005	0.001	0.885	116.84	2.01	0.839	138.9	4.8	big and fat, clear, two terminations, well-defined faces, some inclusions
PM-118-4	309.3	97.5	309.7	89.5	2	10.02	61.32	139.995	0.377	122.54	2.97	85.46	1.44	-	142.6	142.6	31.455	0.085	99.5	1.228	0.030	0.857	0.014	-	0.697	0.697	179.26	3.67	0.812	220.0	9.1	well-defined shape, many inclusions
PM-118-5	275.8	76.9	269.5	85.7	2	6.69	53.37	48.971	0.247	89.33	5.54	51.57	0.72	-	101.4	101.4	7.343	0.037	99.6	0.598	0.037	0.345	0.005	-	0.577	0.577	88.85	4.72	0.786	112.8	12.1	slight rounded terminations, many inclusions

All measure errors of variables were omitted for simplification. Individual age errors are given at 2σ.
Fish Canyon tuff zircons run in conjunction with the first three grains yield a date of 28.9±0.7 Ma (n=4) and with the last two grains, of 28.9±1.9 Ma (n=3).
Np: Number of pyramidal terminations of the grain, used in the alpha ejection correction.
rs: Radius of a sphere with an equivalent surface to volume ratio as the analized crystal.
eU: Effective uranium.
Re: % of total He degassed.
Ft: Alpha ejection correction.
Date It: Age calculated iteratively.

Three ages are in the range 31-35 Ma (early Oligocene). No clear trend is observed between single-grain ZHe ages and effective uranium (Fig. 4).

The five apatite crystals dated are euhedral, with widths >55 μm and lengths <236 μm. Broken ends and corners are present in grains, but have clear faces and are free of inclusions on the microscope (Table 2). Single-grain (U-Th)/He ages range from 10.4±0.6 to 15.1±1.3 Ma, belonging to the middle Miocene. The results give a weighted mean age of 12.1±2.2 Ma (at 95% confidence) with MSWD of 26 (Fig. 5). The single-grain age of 15.1 Ma (PM-116-a01) has low total He degassed (Re=99.1%), suggesting the presence of inclusions or other low-diffusivity zones within the crystal (Table 2). In addition, this date is out of the tendency between single-grain age and effective uranium (eU), displaying high AHe age and low eU value (Fig. 4), which suggests that implantation of alpha particles may have affected the apatite. If this single-grain AHe date is ignored, a slight positive correlation remains between these two variables (Fig. 4). In this case, with four ages, the weighted mean age results of 12.0±2.6 Ma, with a MSWD of 27.

4.1.2. Sample PM-118

The five selected zircon crystals are euhedral, with widths >77 μm and lengths <310 μm. Two terminations and some inclusions are observed (Table 1). They yielded (U-Th)/He ages of 113±12, 139±5, 143±4, 220±9 and 226±10 Ma. The results belong to the Mesozoic and are statistically very scattered, with very low replicability. No correlation is observed between individual crystal ZHe ages and effective uranium (Fig. 4).

The six picked apatites are euhedral crystals, with widths >56 μm and lengths <157 μm. Some crystal show only one termination, but have clear faces and

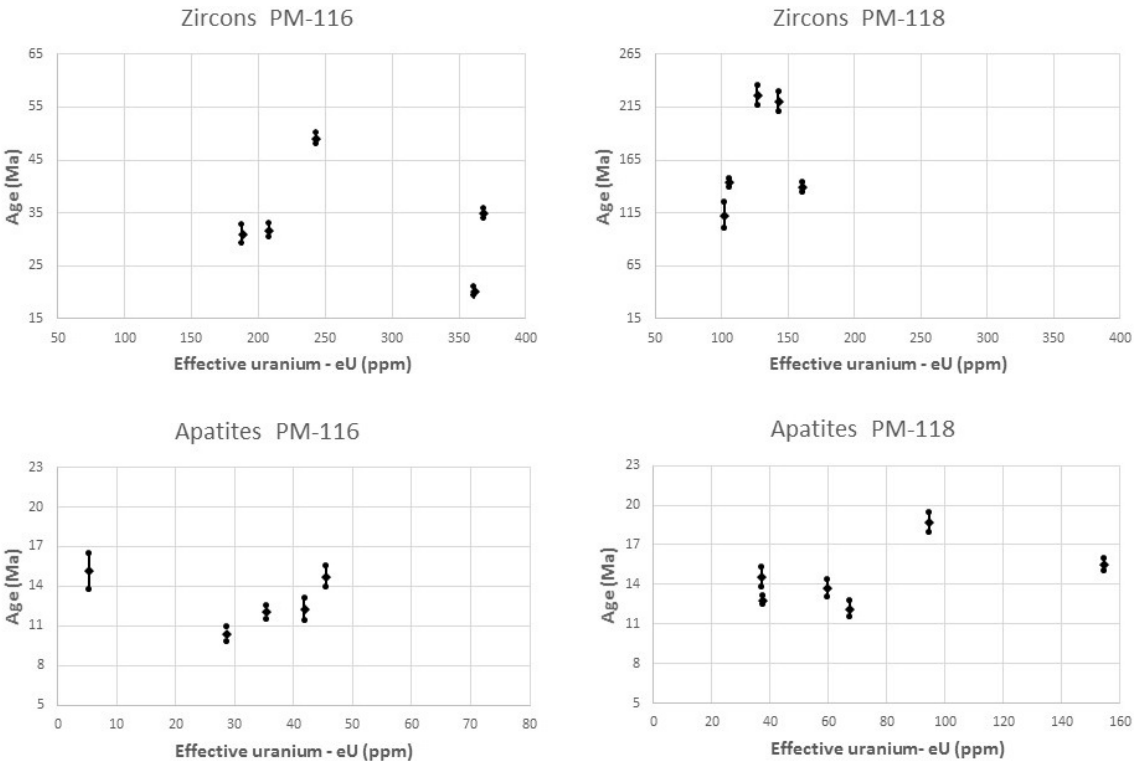

FIG. 4. Plots of the crystal age *versus* effective uranium, for zircons and apatites of the samples PM-116 and PM-118. Note the slight positive correlation for four measures of the apatites of sample PM-116. See text.

TABLE 2. ANALYTICAL DATA OF THE APATITE (U-Th)/He AGES AND CHARACTERISTICS OF THE ANALYZED GRAINS.

Full Sample Name	length 1 (µm)	width 1 (µm)	length 2 (µm)	width 2 (µm)	Np	Dim Mass (µg)	rs (µm)	^{4}He (nmol/g)	±	U (ppm)	±	Th (ppm)	±	Sm (ppm)	±	eU	^{4}He (ncc)	±	Re (%)	U (ng)	±	Th (ng)	±	Sm (ng)	±	Th/U	Raw Date It (Ma)	±	Ft	Corrected Date It (Ma)	Analytic Unc. (Ma)2σ	Notes
PM-116_a01	155.5	114.6	168.1	74.9	0	2.48	42.12	0.284	0.009	3.54	0.19	7.15	0.15	1.98	0.60	5.2	0.016	0.000	99.1	0.009	0.000	0.018	0.000	0.005	0.001	2.023	10.03	0.48	0.662	15.1	1.3	small, broken ends and corners, but crystal faces are clear and inclusions free
PM-116_a02	101.6	104.6	236.2	58.4	1	1.49	35.29	0.961	0.016	20.27	0.74	35.65	0.43	30.32	1.14	28.6	0.032	0.001	100.0	0.030	0.001	0.053	0.001	0.045	0.002	1.759	6.15	0.18	0.587	10.4	0.6	end of a crystal with one broken end, small, no visible inclusions
PM-116_a03	115.7	87.3	108.8	69.6	2	0.84	36.65	1.442	0.018	24.29	0.64	47.62	1.00	51.27	2.58	35.5	0.027	0.000	99.9	0.020	0.001	0.040	0.001	0.043	0.002	1.960	7.43	0.17	0.613	12.0	0.5	small euhedral crystal with no inclusions. A small pock mark on the surface, but pretty
PM-116_a04	107.4	98.6	112.5	68.5	2	0.86	38.07	2.326	0.033	37.68	0.99	33.28	1.84	28.98	1.95	45.5	0.045	0.001	99.9	0.032	0.001	0.029	0.002	0.025	0.002	0.883	9.42	0.25	0.638	14.7	0.8	small, ground end, but otherwise euhedral, clear, inclusions free
PM-116_a05	118.2	76.1	122.5	55.0	2	0.69	32.53	1.597	0.036	31.06	1.09	46.35	1.50	31.46	2.43	42.0	0.025	0.001	99.9	0.021	0.001	0.032	0.001	0.022	0.002	1.492	7.00	0.24	0.568	12.3	0.8	nice small crystal, long, no inclusions, one missing corner but clear and euhedral
Weighted mean age, sample PM-116: 12.1±2.2 Ma (MSWD=26)																																
PM-118_a01	145.7	110.2	145.7	139.6	1	4.05	59.26	1.983	0.012	27.79	0.46	41.61	0.38	12.70	0.45	37.6	0.180	0.001	100.0	0.113	0.002	0.169	0.002	0.051	0.002	1.497	9.74	0.13	0.760	12.8	0.3	medium, ground, clear, nice crystal faces, only one termination, no inclusions
PM-118_a02	156.7	89.0	151.0	72.8	2	1.44	41.59	2.915	0.025	41.85	1.31	76.36	1.83	20.83	1.12	59.8	0.094	0.001	100.0	0.060	0.002	0.110	0.003	0.030	0.002	1.825	8.99	0.21	0.654	13.7	0.6	beautiful crystal, euhedral, no inclusions
PM-118_a03	144.2	85.8	142.1	67.2	1	1.42	38.56	1.861	0.031	26.78	0.73	44.32	0.75	14.68	1.08	37.2	0.059	0.001	100.0	0.038	0.001	0.063	0.001	0.021	0.002	1.655	9.23	0.24	0.632	14.6	0.7	one ground down end, one termination, no inclusions, some surface chips
PM-118_a04	127.0	79.0	131.7	56.0	2	0.79	33.65	5.518	0.053	60.51	1.63	145.46	2.36	22.92	2.07	94.7	0.098	0.001	100.0	0.048	0.001	0.116	0.002	0.018	0.002	2.404	10.75	0.22	0.574	18.7	0.7	beautiful little crystal, clear, well formed
PM-118_a05	82.4	80.8	82.4	72.6	1	0.76	33.75	2.628	0.034	47.83	1.53	82.77	1.46	26.82	1.96	67.3	0.045	0.001	100.0	0.036	0.001	0.063	0.001	0.020	0.001	1.730	7.20	0.19	0.591	12.2	0.6	end of a crystal, one termination, clear, fat, no inclusions
PM-118_a06	82.2	71.4	81.7	62.8	2	0.41	29.07	6.793	0.081	100.77	1.69	228.13	3.74	59.12	3.96	154.4	0.062	0.001	100.0	0.041	0.001	0.093	0.002	0.024	0.002	2.264	8.11	0.14	0.521	15.5	0.5	little crystal, fat, very clear, no inclusions
Weighted mean age, sample PM-118: 14.0±2.1 Ma (MSWD=60) or 13.6±1.7 Ma (MSWD=28, without PM-118-a04)																																

All measure errors of variables were omitted for simplification. Individual age errors are given at 2σ.
Shards of Durango fluorapatite run in conjunction with these grains yield a date of 31.5±0.4 Ma (n=6).
Np: Number of pyramidal terminations of the grain, used in the alpha ejection correction.
rs: Radius of a sphere with an equivalent surface to volume ratio as the analized crystal.
eU: effective uranium.
Re: % of total He degassed.
Ft: Alpha ejection correction.
Date It: Age calculated iteratively.

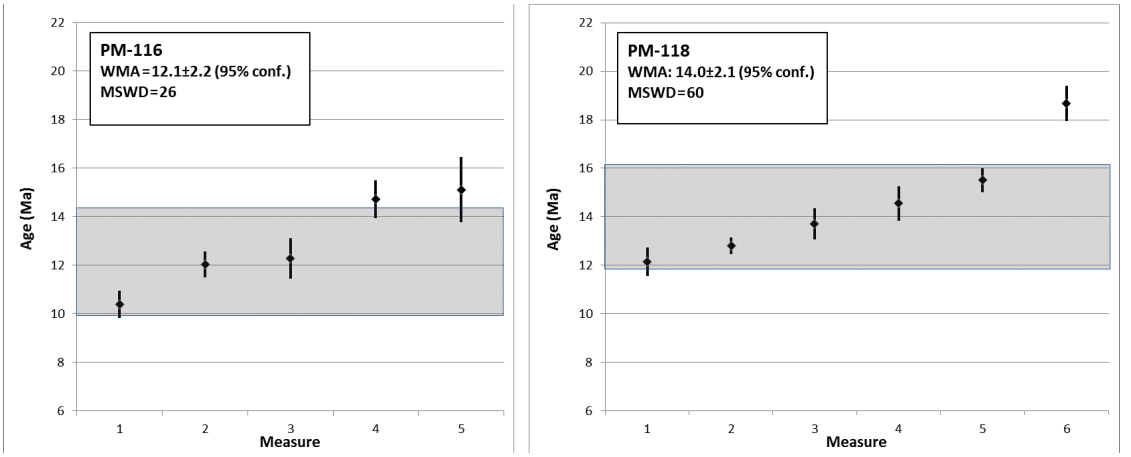

FIG. 5. Plots of the apatite (U-Th)/He ages and weighted mean ages (WMA) for samples PM-116 and PM-118. The grain ages are ordered from least to greatest and the gray band indicates the range of the weighted mean age.

are free of inclusions on the microscope (Table 2). The (U-Th)/He measures in these grains generated individual ages from 12.2±0.6 to 18.7±0.7 Ma, *i.e.*, from the early-middle Miocene. The crystals produce a weighted mean of 14.0±2.1 Ma (at 95% confidence) with MSWD of 60 (Fig. 5). No correlation exists between the single-grain age and eU (Fig. 4). Four ages at 12.2 to 14.6 Ma are observed with relatively similar eU (37.2-67.3 ppm). The individual crystal PM-118-a04 displays relatively high eU and higher AHe age (18.7 Ma; Fig. 4 and Table 2); it is the only that does not overlap with the weighted mean age within errors (Fig. 5). If this crystal date is ignored, the weighted mean age results of 13.6±1.7 Ma with MSWD of 28.

4.2. Inverse thermal models

Because zircons on both samples display visibly inclusions and high dispersion of their ZHe ages, these data were not included in the thermal modeling. Four out of five AHe ages of the sample PM-116 show a slight positive correlation between single-grain age and effective uranium (Fig. 4), that suggests this sample has undergone a relatively slow cooling. The T-t model with these measures indicates a wide range of possible thermal paths. The more probable path shows slow cooling from 15 to 0 Ma, that left the rock below 20 ºC. A relatively more marked cooling period, from 80 to 50 °C, is observed at 11-7 Ma (Fig. 6A).

5. Discussion

The ZHe ages in one sample are from 113 to 226 Ma, whereas in the other sample are from 20 to 49 Ma. These extremely different ages are related to the inclusion abundance and possible zoning in crystals. Zoning and heterogeneities in zircons of the BMC rocks have been reported by Wörner *et al*. (2000a), Loewy *et al*. (2004) and Arcos *et al*. (2016). Therefore, the geological interpretation of the ZHe ages is not possible. The AHe ages reported here for the BMC rocks (from 10.4 to 18.7 Ma) are similar to AHe and AFT ages (from 11 to 13 Ma) obtained by Horton *et al.* (2006) for the same rocks. Both studies are the unique that present AHe ages in the Western Cordillera of the Altiplano (14-22° S). Unfortunately, the work of Horton *et al.* (2006) is an abstract and the analytical data, ages, errors and modeling are not available, and integration and discussion of data are not possible.

The sample PM-116 gives an AHe weighted mean age of 12.1±2.2 Ma (MSWD=26), and the PM-118, 14.0±2.1 Ma (MSWD=60). For the sample PM-116, if the higher single-grain age of 15.1 Ma (PM-116-a01) is ignored by low Re, the weighted mean age results of 12.0±2.6 Ma with a MSWD of 27. For the sample PM-118, if the higher single-grain age of 18.7 Ma is ignored, the weighted mean age results of 13.6±1.7 Ma with a MSWD of 28, a value considerably lower than 60. In any cases, the MSWDs of 26-28 are high and data fail

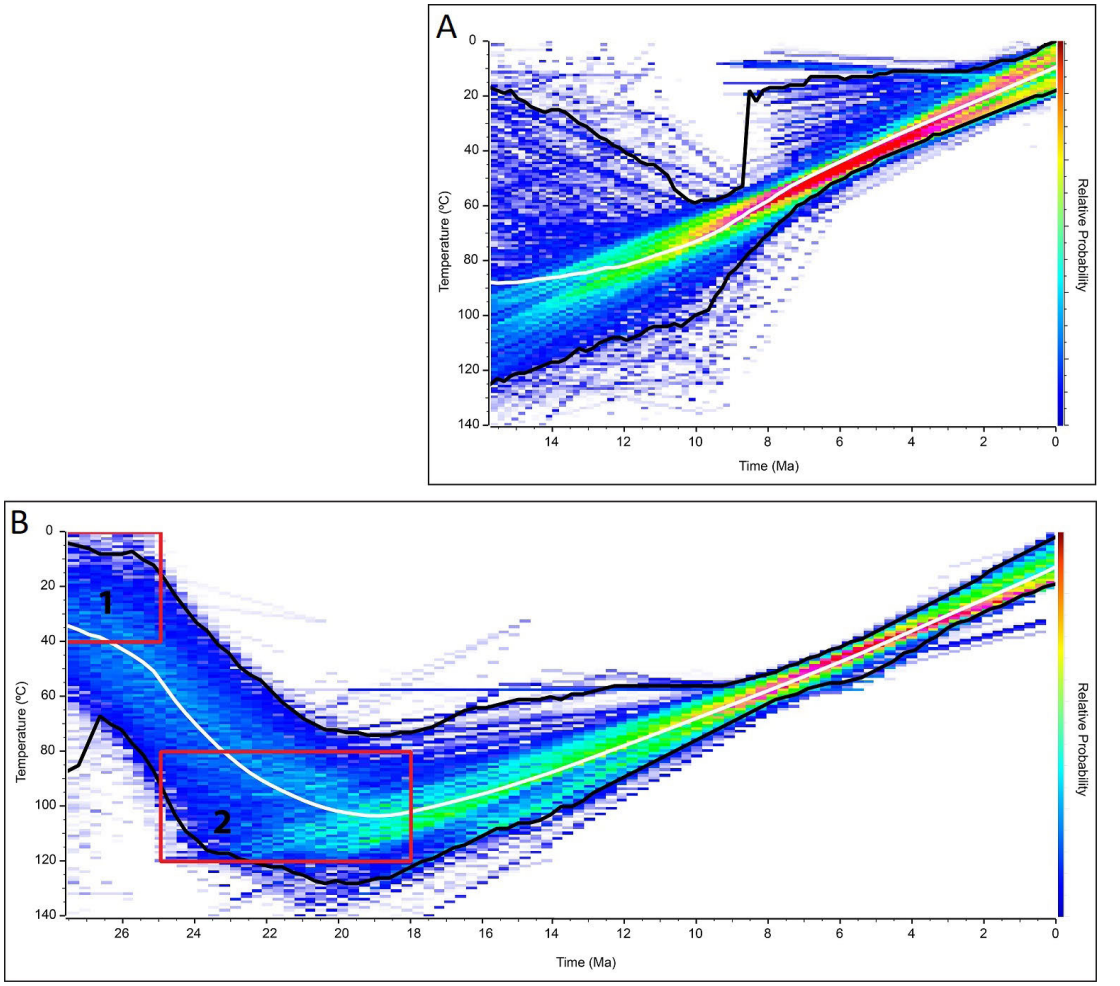

FIG. 6. **A** and **B** Inverse thermal models from the four selected ages of the sample PM-116 (see text), using the QTQt v 5.6.0 software (Gallagher, 2012). The withe line shows the most probable path whereas the black lines, the range of this path. In **B**, the red squares indicate geological constraint points: (**1**) 20±20 °C at 27.5±2.5 Ma considering as the exposition period of the Belén Metamorphic Complex; and (**2**) 100±20 °C at 21.5±3.5 Ma, as the burial period provoked by the Lupica Formation deposition over the BMC and associate volcanic activity.

the chi-square test, thus, the weighted mean ages should be viewed with caution.

The slight positive correlation between single-grain AHe age and eU for four selected mesures in sample PM-116 suggests that the rock cooled slowly. We explore models considering geological constraints in the thermal history of the BMC: (**1**) rock temperature near to the surface of 20±20 °C at 27.5±2.5 Ma, as the exposition period of the BMC, and (**2**) rock temperature of 100±20 °C at 21.5±3.5 Ma, as the burial period provoked by the Lupica Formation deposition (2,500 m thickness) over the BMC and associate volcanic activity (FIG. 6B). If the geological constraints are added, the paths of T-t model between 15 and 0 Ma become more restricted compared to the T-t model without geological constraints (FIG. 6A). In this case, slow heating at 27-19 Ma and slow cooling after 15 Ma are more defined. The T-t modeling performed without geological constraints shows a slow cooling from 15 to 0 Ma, with a relatively more marked cooling period at 11-7 Ma. This is compatible with exhumation induced by tectonism and would permit to date the last activity of the Chapiquiña-Belén reverse fault, which uplifted the

BMC block. The age agrees with exhumation age of the BMC by erosion, contractional deformation and uplift affecting the Western Cordillera and dated by stratigraphy and cross-cutting relationships from 18 to 6 Ma (García *et al*., 2004; Charrier *et al.*, 2013). Additionally, the exhumation period coincides in part with the deformation causing the Oxaya anticline in the Precordillera at this latitude, dated between *ca*. 11.7 and 10.7 Ma (García and Hérail, 2005; García *et al.*, 2017).

The middle-late Miocene thermal signal of this part of the Western Cordillera is relatively similar to that the eastern Altiplano (Eastern Cordillera and Subandean belt), according the AFT and AHe data reported there (Gillis *et al*., 2006; Ege *et al.*, 2007; Barnes *et al*., 2012; McQuarrie *et al*., 2008; Perez *et al*., 2016; Anderson *et al*., 2018). However, this signal differs considerably from that the forearc (from the Coastal Cordillera to Precordillera) and the eastern Western Cordillera. At this latitude, in the first domain (forearc), the available AHe ages are from 24±8 to 43±4 Ma (Avdievitch *et al*., 2018), AFT ages are from 37±3 to 123±7 Ma (Schlunegger *et al.,* 2006), and models indicates an extremely low exhumation rate, while in the second domain (eastern Western Cordillera, Uyarani basement), the available AHe and AFT ages are greater than 34 Ma (Horton *et al.*, 2006; Barnes *et al*., 2012). The last ages are compatible with the early Oligocene exposition of the BMC and the Incaic orogeny that affected the arc and inner forearc (Steinman, 1929; Mégard, 1987; Noblet *et al*., 1996; Maksaev and Zentilli, 1999; Charrier *et al*., 2013; García *et al.*, 2017). This suggests that during the Miocene the cooling-uplift of the western part of the Western Cordillera was coupled to the eastern Altiplano and decoupled from the forearc and eastern Western Cordillera. In contrast, before 18 Ma, in particular during the Incaic orogeny, the exhumation of the Western Cordillera seems to have coupled to the forearc. More (U-Th)/He analyses in the BMC and other geological units, and more thermo-chronometers, are needed to more robust conclusions on the exhumation and burial history of the Western Cordillera.

Note that 450 km south of the study area, in the Salar de Atacama basin (23-24° S), Oligocene-lower Miocene localized extension has been documented, probably associated with transtensional movements (Pananont *et al*., 2004; Jordan *et al*., 2007). This is apparently contradictory with the observed in our study area and surroundings. Higher precision on the age of the Oligocene (*s.l.*) events at 18-19° S and 23-24° S is necessary for correlation, as well as improved refinement on the spatial association between these different Andean segments.

6. Conclusions

The ZHe ages of the sample PM-118 belong to the Mesozoic, from 113 to 226 Ma, whereas the sample PM-116 yielded ZHe ages of the Paleogene, from 20 to 49 Ma, with three values at 31-35 Ma. The extremely different ages are related to inclusions and zoning in crystals, thus, their geological meaning is not clear.

The 11 AHe ages range from 10.4 to 18.7 Ma. The positive correlation between single-grain AHe age and eU in sample PM-116 suggests that the rock slowly cooled. The T-t modeling performed with the selected measures of sample PM-116 shows a slow cooling from 15 to 0 Ma, with a relatively more marked cooling period at 11-7 Ma. This is compatible with exhumation induced by tectonism and would permit to date the last activity of the Chapiquiña-Belén reverse fault that uplift the BMC rocks. The exhumation age agrees with period of contractional deformation and uplift dated independently from 18 to 6 Ma.

The middle-late Miocene thermal signal of the western part of the Western Cordillera is relatively similar to that the Eastern Cordillera and Subandean belt, and differs considerably from that the forearc (Coastal Cordillera to Precordillera) and eastern Western Cordillera. This suggests that during the Miocene the cooling-uplift of the western part of the Western Cordillera was decoupled from the forearc. In contrast, before 18 Ma, in particular during the Incaic orogeny, the exhumation of the Western Cordillera would have been coupled to the forearc.

Acknowledgments

This work resulted from a collaborative initiative between the AMTC-Universidad de Chile (ANID/PIA Project AFB180004) and Chilean Servicio Nacional de Geología y Minería (SNGM), in the context of the Geological Survey of the 1:100.000 scale Putre sheet. We thank especially to geologist M. Ladino from the SNGM for his interest in this study and collaboration. We thank to K. Gallagher for the access of QTQt v 5.6.0 (2017) program to infer thermal histories from low temperature

thermochronology. Fructiferous discussions were held with colleagues A. Tomlinson and M. Farías. Edition of this paper was made by F. Martínez and W. Vivallo.

References

Arcos, R.; Naranjo, J.A.; Ladino, M. ; Polanco, E. 2016. Carta Putre, Región de Arica y Parinacota. Servicio Nacional de Geología y Minería. Carta Geológica de Chile, Serie Geología Básica 197: 141 p., 1 mapa escala 1:100.000.

Anderson, R.B.; Long, S.P.; Horton, B.K.; Thomson, S.N.; Calle, A.Z.; Stockli, D.F. 2018. Orogenic wedge evolution of the central Andes, Bolivia (21°S): Implications for Cordilleran cyclicity. Tectonics 37: 3577-3609. doi: 10.1029/2018TC005132.

Avdievitch, N.; Ehlers, T.; Glotzbach, C. 2018. Slow Long-Term Exhumation of the West Central Andean Plate Boundary, Chile. Tectonics 37: 2243-2267. doi: 10.1029/2017TC004944.

Barnes, J.B.; Ehlers, T.A.; Insel, N.; McQuarrie, N.; Poulsen, C.J. 2012. Linking orography, climate, and exhumation across the central Andes. Geology 40 (12): 1135-1138.

Basei, M.A.; Charrier, R.; Hervé, F. 1996. New ages (U-Pb, Rb-Sr, K-Ar) from supposed Pre-cambrian units in northern Chile: Some geotectonic implications. *In* International Symposium on Andean Geodynamics (ISAG), No. 3: 763-766. Saint Malo, France.

Charrier, R.; Hérail, G.; Pinto, L.; García, M.; Riquelme, R.; Farías, M.; Muñoz, N. 2013. Cenozoic tectonic evolution in the Central Andes in northern Chile and west central Bolivia: implications for paleogeographic, magmatic and mountain building evolution. International Journal of Earth Science 102 (1): 235-264.

Damm, K.; Russell, H.; Kelley, S. 1994. Some isotopic and geochemical constraints on the origin and evolution of the central Andes Basement (19°-24°S). *In* Tectonics of the Southern Central Andes (Reutter, K-J.; Scheuber, E.; Wigger, P.; editors). Springer-Verlag: 263-276. Berlin.

Ege, H.; Sobel, E.R.; Scheuber, E.; Jacobshagen, V. 2007. Exhumation history of the southern Altiplano plateau (southern Bolivia) constrained by apatite fission track thermochronology. Tectonics 26: TC1004. doi: 10.1029/2005TC001869.

Ehlers, T.A.; Farley, K.A. 2003. Apatite (U-Th)/He thermochronometry: methods and applications to problems in tectonic and surface processes. Earth and Planetary Science Letters 206: 1-14. doi: 10.1016/S0012-821X(02)01069-5.

Gallagher, K. 2012. Transdimensional inverse thermal history modelling for quantitative thermochronology. Journal of Geophysical Research 117: B02408. doi: 10.1029/2011JB00882.

García, M.; Hérail, G. 2005. Fault-related folding, drainage network evolution and valley incision during the Neogene in the Andean Precordillera of Northern Chile. Geomorphology 65 (3-4): 279-300.

García, M.; Gardeweg, M.; Clavero, J.; Hérail, G. 2004. Hoja Arica, Región de Tarapacá. Servicio Nacional de Geología y Minería. Carta Geológica de Chile: 150 p., 1 mapa escala 1:250.000.

García, M.; Maksaev, V.; Townley, B.; Dilles, J. 2017. Metallogeny, structural evolution, post-mineral cover distribution and exploration in concealed areas of the northern Chilean Andes. Ore Geology Reviews 86: 652-672.

Gillis, R.J.; Horton, B.K.; Grove, M. 2006. Thermochronology, geochronology, and upper crustal structure of the Cordillera Real: Implications for Cenozoic exhumation of the central Andean plateau. Tectonics 25: TC6007. doi: 10.1029/ 2005TC001887.

Hiess, J.; Condon, D.J.; Mclean, N.; Noble, S.R. 2012. $^{238}U/^{235}U$ Systematics in Terrestrial Uranium-Bearing Minerals. Science 335: 1610-1614. doi: 10.1126/science.1215507.

Horton, B.; Gillis, R.; Farley, K.; Wörner, G. 2006. Cenozoic Exhumation of the Margins of the Central Andean Plateau: Results from Low Temperature Thermochronology and Synorogenic Stratigraphy. American Geophysical Union, Fall Meeting, Abstract: id. 2006AGUFM.T44A.08H.

Jordan, T.E.; Mpodozis, C.; Muñoz, N.; Blanco, N.; Pananont, P.; Gardeweg, M. 2007. Cenozoic subsurface stratigraphy and structure of the Salar de Atacama Basin, northern Chile. Journal of South American Earth Sciences 23: 122-146. doi: 10.1016/j.jsames.2006.09.024.

Ketcham, R.A.; Gautheron, C.; Tassan-Got, L. 2011. Accounting for long alpha-particle stopping distances in (U-Th-Sm)/He geochronology: Refinement of the baseline case. Geochmica Et Cosmochimica Acta 75 (24): 7779-7791. doi: 10.1016/j.gca.2011.10.011.

Loewy, S.; Connelly, J.; Dalziel, I. 2004. An orphaned basement block: The Arequipa-Antofalla basement of the central Andean margin of South America. Geological Society of America Bulletin 116: 171-187.

Ludwig, K. 2012. User's manual for Isoplot version 3.75-4.15: A geochronological toolkit for Microsoft, Excel. Berkley Geochronological Center Special Publication 5: 75 p.

Maksaev, V.; Zentilli, M. 1999. Fission track thermochronology of the Domeyko Cordillera, northern Chile: implications for Andean tectonics

and porphyry copper metallogenesis. Exploration and Mining Geology 8: 65-89.

McQuarrie, N.; Barnes, J.B., Ehlers, T.A. 2008. Geometric, kinematic, and erosional history of the central Andean Plateau, Bolivia (15-17°S). Tectonics 27 (3): 999-1002. doi: 10.1029/2006TC002054.

Mégard, F. 1987. Cordilleran Andes and marginal Andes: a review of Andean geology north of the Arica elbow (18ºS). *In* Circum-Pacific Orogenic Belts and Evolution of the Pacific Basin (Monger, J.W.H.; Francheteau, J.; editors). American Geophysical Union, Geodynamic Series 18: 71-95.

Muñoz, N.; Charrier, R. 1996. Uplift of the western border of the Altiplano on a west-vergent thrust system, Northern Chile. Journal of South American Earth Sciences 9 (3-4): 171-181.

Murray, K.E.; Braun, J.; Reiners, P.W. 2018. Toward robust interpretation of low-temperature thermochronometers in magmatic terranes. Geochemistry, Geophysics, Geosystems 19 (10): 3739-3763.

Noblet, C.; Lavenu, A.; Marocco, R. 1996. Concept of continuum as opposed to periodic tectonism in the Andes. Tectonophysics 255 (1-2): 65-78.

Pacci, D.; Hervé, F.; Munizaga, F.; Kawashita, K.; Cordani, U.; 1980. Acerca de la edad Rb/Sr precámbrica de rocas de la Formación Esquistos de Belén, Departamento de Parinacota, Chile. Revista Geológica de Chile 11: 43-50. doi: 10.5027/andgeoV7n3-a03.

Pananont, P.; Mpodozis, C.; Blanco, N.; Jordan, T.E.; Brown, L.D. 2004. Cenozoic evolution of the northwestern Salar de Atacama Basin, northern Chile. Tectonics 23: TC6007. doi: 10.1029/2003TC001595.

Perez, N.D.; Horton, B.K.; McQuarrie, N.; Stübner, K.; Ehlers, T.A. 2016. Andean shortening, inversion and exhumation associated with thin- and thick-skinned deformation in southern Peru. Geological Magazine 153: 1013-1041.

Pinto, L.; Hérail, G.; Fontan, F.; Parseval, P. 2007. Neogene erosion and uplift of the western edge of the Andean Plateau as determined by detrital heavy mineral analysis. Sedimentary Geology 195: 217-237.

Reiners, P.W.; Ehlers, T.A.; Zeitler, P.K. 2005. Past, present, and future of thermochronology. Review in Mineralogy and Geochemistry 58 (1): 1-18.

Salas, R.; Kast, R.; Montecinos, F.; Salas, I. 1966. Geología y recursos minerales del Departamento de Arica, Provincia de Tarapacá. Instituto de Investigaciones Geológicas, Boletín 21: 130 p.

Schildgen, T.F.; Hodges, K.V.; Whipple, K.X.; Reiners, P.W.; Pringle, M.S. 2007. Uplift of the western margin of the Andean plateau revealed from canyon incision history, southern Peru. Geology 35 (6): 523-526.

Schlunegger, F.; Zeilinger, G.; Kouno, A.; Kober, F.; Hüsser, B. 2006. Scale of relief growth in the forearc of the Andes of Northern Chile (Arica latitude, 18°S). Terra Nova 18: 217-223.

Steinmann, G. 1929. Geologie von Peru. Carl Winters Universitätsbuchhandlung: 448 p. Heidelberg.

Wotzlaw, J.; Decou, A.; von Eynatten, H.; Wörner, G.; Frei, D. 2011. Jurassic to Palaeogene tectono-magmatic evolution of northern Chile and adjacent Bolivia from detrital zircon U-Pb geochronology and heavy mineral provenance. Terra Nova 23: 399-406.

Wörner, G.; Lezaun, J.; Beck, A.; Heber, V.; Lucassen, F.; Zinngrebe, E.; Rössling, R.; Wilke, H.G. 2000a. Precambrian and Early Paleozoic evolution of the Andean basement at Belén (northern Chile) and Cerro Uyarani (western Bolivia Altiplano). Journal of South American Earth Sciences 13 (8): 717-737.

Wörner, G.; Hammerschmidt, K.; Henjes-Kunst, F.; Lezaum, J.; Wilke, H. 2000b. Geochronology ($^{40}Ar/^{39}Ar$, K-Ar and He-exposure ages) of Cenozoic magmatic rocks from northern Chile (18-22°S): Implications for magmatism and tectonic evolution of the central Andes. Revista Geológica de Chile 27 (2): 205-240. doi: 10.5027/andgeoV27n2-a04.

Manuscript received: June 17, 2021; revised/accepted: January 19, 2022; available online: May 31, 2022.
Editorial handling: Waldo Vivallo